HNPS Advances in Nuclear Physics

Vol 5 (1994)

HNPS1994

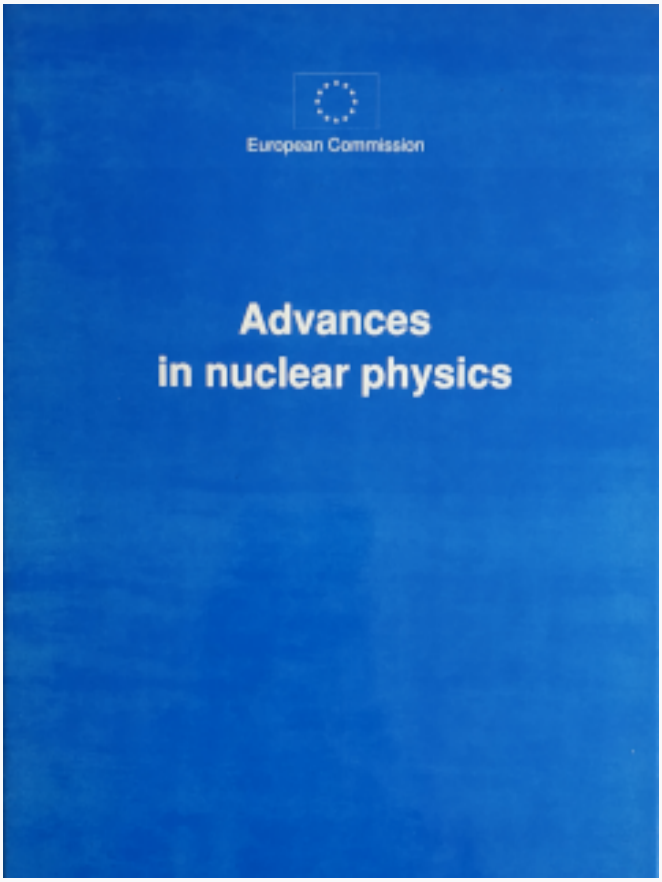

Materials analysis by ion channeling at "Demokritos"

S. Harissopulos, S. Kossionides, T. Paradellis, G. Maggiore

doi: 10.12681/hnps.2904

Materials analysis by ion channeling at "Demokritos"

S. HARISSOPULOS, S. KOSSIONIDES, and T. PARADELLIS
Institute of Nuclear Physics, N.C.S.R. "Demokritos"
GR-15310 Aghia Paraskevi, Attiki, Greece
and
C. MAGGIORE
Center for Materials Science, Los Alamos National Laboratory,
Los Alamos, NM 87545, USA

Abstract

A new fully automated Goniometer system installed recently at the Institute of Nuclear Physics of "Demokritos" is presented. This system enables to perform materials analysis not only via the Rutherford Backscattering method, which has been used so far at "Demokritos", but also by the ion channeling technique. The first experiments carried out using the Goniometer are also presented.

Presented by S. Harissopulos.

1 Introduction in channeling and its applications

One of the "classic" nuclear techniques to perform materials analysis is the Rutherford Backscattering method (RBS); This method has been used widely and very extensively over the past 20 years. As shown in fig. 1a, in an RBS experiment a beam of ions of mass M_1 and atomic number Z_1, having a kinetic energy E_0 in the $0.5 - 5\ MeV$ range, impinges on a "thick" sample of material (target) of mass M_2 and atomic number Z_2. The beam particles are then scattered by the target atoms. When counting the number of the ions scattered into a solid angle $d\Omega$ covered by the surface of a detector, one obtains the spectrum shown in fig. 1a. The energy of the scattered particles is continiously distributed in the range 0 to E_s, where E_s is given by eq. 1.

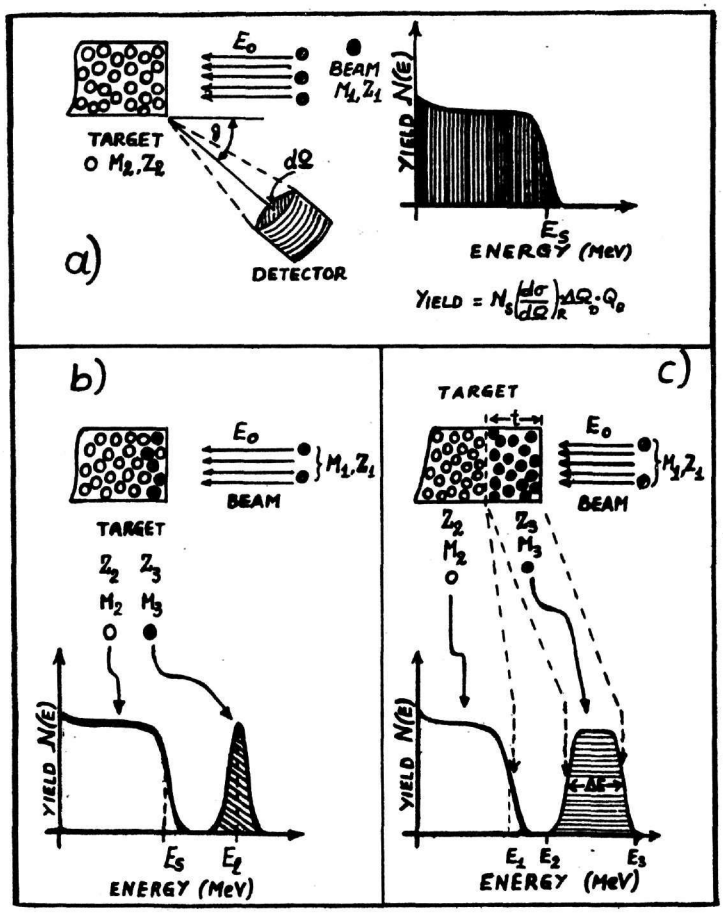

FIG. 1: Principle of the RBS method.

$$E_s = E_0 \cdot K^2, \qquad K = \frac{M_1 cos\theta}{M_1 + M_2} + \sqrt{\left(\frac{M_1 cos\theta}{M_1 + M_2}\right)^2 + \frac{M_2 - M_1}{M_1 + M_2}} \qquad (1)$$

Hereby, θ is the scattering angle. The yield $N(E)$ at E_s provides the number of the particles scattered by the target atoms on the target surface. A portion of the beam penetrates into the target and it is scattered while losing kinetic energy continiously down to $E = 0$. The spectrum shown in fig. 1b is obtained when a thin layer of atoms of atomic number Z_3 and mass M_3 covers the "thick" sample. This layer gives rise to a "peak" of energy E_l corresponding to the portion of the beam particles scattered by the thin layer on the surface. According to eq. (1), if $M_3 > M_2$ then the latter peak lies on the right of E_s, i.e. $E_l > E_s$, and vice versa. By increasing the thickness of the layer the width of the peak increases as well, and the spectrum looks like this shown in fig 1c. Hence: **In an RBS measurement, the number of the atoms N_s of the extra layer and its thickness t can be obtained from the yield $N(E)$ and the "width" ΔE, respectively.**

The channeling method, which is illustrated in fig. 2, is based on the steering of the

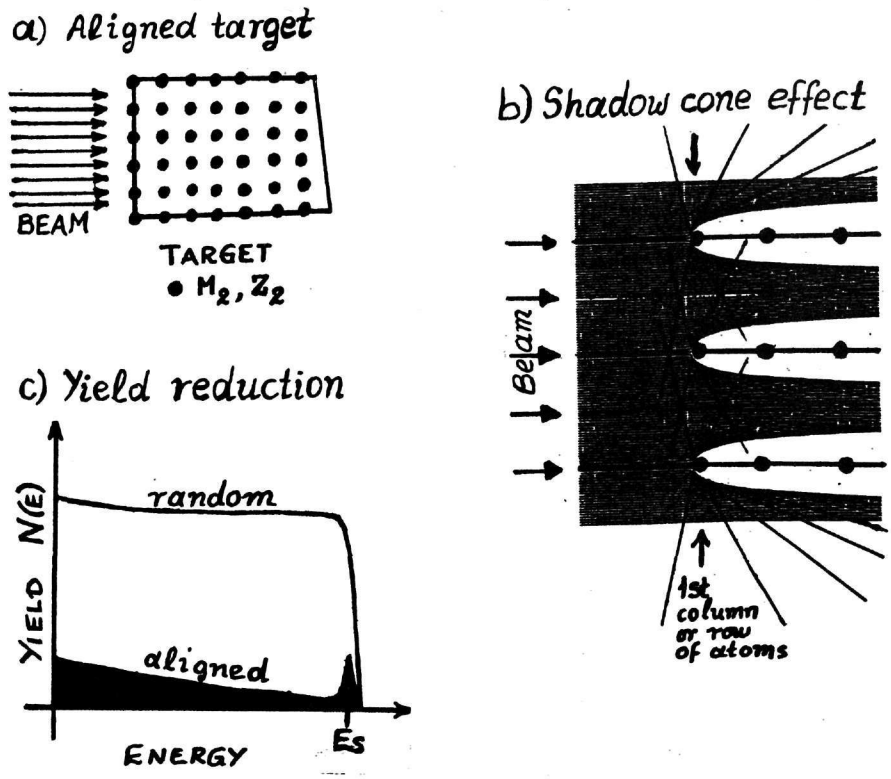

FIG. 2: Principle of Channeling

beam particles into the open spaces (channels) between closed packed rows or planes of atoms in a crystal. This effect is the result of a correlated series of small-angle screened Coulomb collisions between a beam particle and the atoms bordering the channel. As shown in fig. 2a, channeling occurs when the crystal is "well aligned" to the beam direction. Then the impinging ions are scattered by the target atoms of *only* the "first" row (or column) of the crystal lattice. As it is shown in fig. 2b, these "front" atoms shield the rest atoms of the next row (or column). When the beam particles are "channeled" into the open spaces between two rows (or columns) of atoms, they do not penetrate closer than the screening distance to the atomic nuclei. Hence, the probability of large angle Rutherford back-scattering is signifficantly reduced. Consequently, **when channeling occurs the yield of beam particles scattered at a certain angle, i.e. the counting rate, is lower than this observed when bombarding the target randomly.** A "channeled" spectrum is schematically compared to a "random" one in fig. 2c. The small "surface peak" shown in the channeled case of a perfect oxide-free crystal is due to the scattering from the outermost layer of atoms, which are not shadowed.

The fraction

$$\chi = \frac{Y_C}{Y_R} \tag{2}$$

of the channeled yield Y_C to the random one Y_R is actually the main experimental quantity measured in a channeling experiment. Fraction χ is usually called *normalized yield*. The better the crystal is aligned the smaller the value of χ is. For the most favourable cases χ can be reduced down to 0.01. for a perfect crystal.

Fig. 3 illustrates further the most important feature of channeling: As shown in this

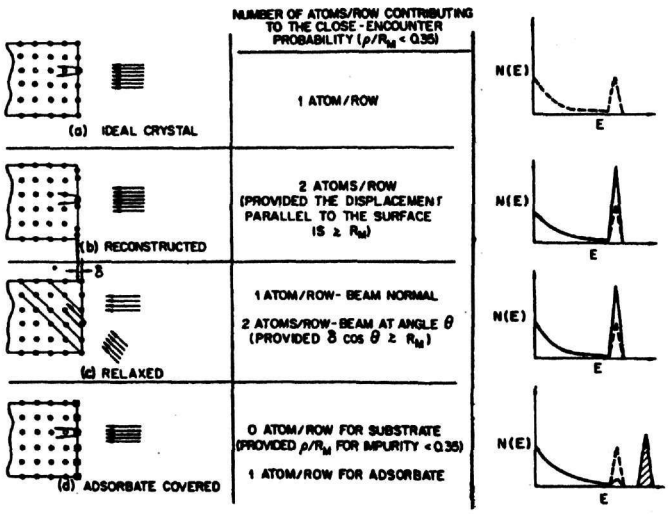

FIG. 3: Channeling spectra of non-perfect crystals. Case a): ideal crystal. In cases b) and c) the crystal is reconstructed and relaxed respectively. Both effects lied to an increase of the surface peak measured in case a). In case d) the surface peak is decreased and a second peak at higher energy arises (from ref. [1]).

fig., χ **is increased also when the crystal is properly aligned, but the crystal lattice is somehow "perturbed"**, i.e. when damages, defects, impurities etc. are "present". This fact is the basis of the application of the channeling technique to the materials analysis.

Channeling can be applied in many cases of materials analysis. Two such cases, which are very important in the modern materials science, are a) the surface layers and interfaces and b) the epitaxial systems. Both cases can be analyzed, as briefly shown below, via RBS-Channeling.

The case of surface layers is illustrated in fig. 4. In this figure ion scattering spectra for an amorphous film on single-crystal substrates are shown. In case a) of fig. 4, the

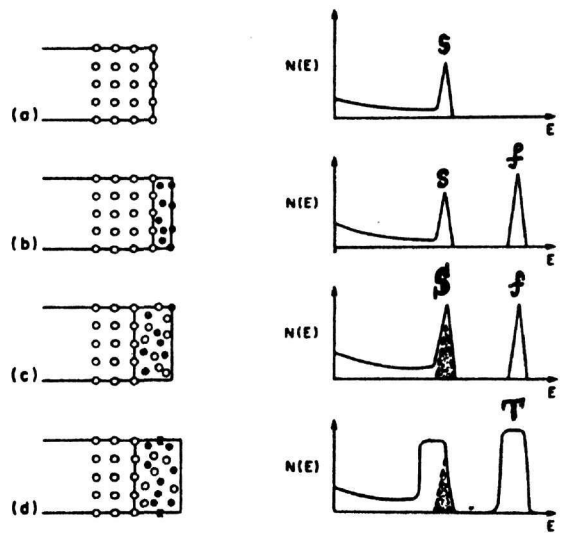

FIG. 4: Channeling spectra for amorphous film on single-crystal substrates. o:=atoms of crystal with mass M_2. •:=atoms of the deposited layer of mass M_3. ($M_3 > M_2$). (From ref. [1]).

spectrum shown there,is the channelled spectrum of an "uncovered" crystal, which consists of atoms of mass M_2 and has an ideal or bulk-like surface. The peak labeled "s" is due to the ion scattering on the surface atoms (*surface peak*). Spectrum of case b) is obtained when the crystal is covered with a "passive" thin film consisted of atoms of mass $M_3 > M_2$. The latter spectrum "includes" spectrum of case a) and a second peak, labeled "f", which arises from the ion scattering on the atoms of the thin film. When the single-crystal is covered with a thin "active" film, which reacts with the crystal to form a thin layer composed of atoms of mass M_3 and M_2 ($M_3 > M_2$), then one obtains the spectrum shown in case c) of fig. 4. By comparing spectra of c) and b), it can be seen that the peak "s" has become broader (peak "S"), whereas peak labelled "f" has not been changed. In addition, both peaks have almost the same "height". The latter two peaks "S"and "f" of case c) become trapezoids as shown in case d), when the "active" film becomes thick. In all above cases of surface layers, the thickness of the films can be determined from the width of the peak "f" or the trapezoid "T" and the increase of the width on the peak "s".

The case of epitaxial systems, i.e. systems which consist of two or more crystals in contact with a specific crystallographic orientational relationship, is illustrated in fig. 5. In case a) of fig. 5 are shown an ideal homoepitaxial system as well as the respective channeled spectrum measured for such an ideal system. In this spectrum a small surface-peak labeled "s" is to be seen. In case b), an epitaxial layer with disorder at the crystal-crystal interface gives rise to a second "broad" peak, labeled "d" at lower energy. In comparison to spectrum of case a), the normalized yield $N(E)$ is here increased all over the spectrum. From the energy difference of the centroids of the peaks "s" and "d", the distance of the disordered region from the surface can be estimated. Furthermore, from the width of peak "d" the width of the disordered region can be derived. In a "textured" polycrystalline film of case c), the surface peak "s" is replaced by a broad trapezoid labeled "t". The yield $N(E)$ is also here increased all over the spectrum. In case d), i.e. the case of a radomly oriented polycrystalline or amorphous film, the surface peak "s" is also replaced by a trapezoid labeled "T". When comparing case d) with case c) one can easily find that in the former case the normalized yield reaches the value of that measured in a random run, i.e $N(E) = 1$. From the width of the trapezoids "t" and "T", the "depths" of the misoriented and the amorphous region respectively can be determined.

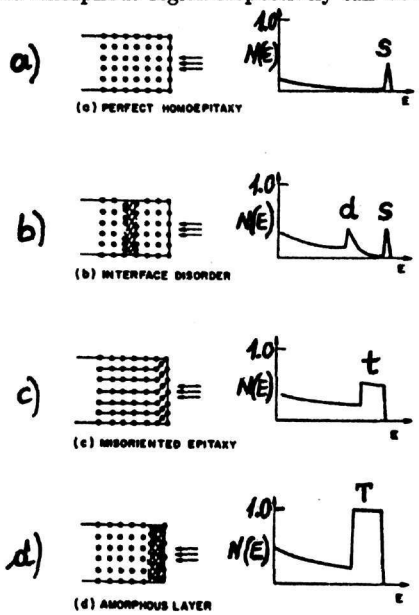

FIG. 5: Channeling spectra of epitaxial systems (from ref. [1]).

Via channeling one can also perfom very sensitive crystallographic studies. This can be illustrated quantitatively by means of the so-called angular scan plots shown in fig. 6. In an angular scan, one determines the normalized yield χ at very small tilt angles ψ defined by the beam axis and the "channel axis" of the crystal. As shown in fig. 6 the form of the angular scan plot depends e.g. on the position of a solute atom of a

lattice in the projection into an axial channel. As illustrated in case a) of fig. 6, when solute atoms do not project into the channel, the profiles of solute and host atoms are identical. In case b), i.e. small displacements into the the channel, the dip in yield from host atoms is broader than that of solute atoms. For large displacements of $\approx 0.1nm$,

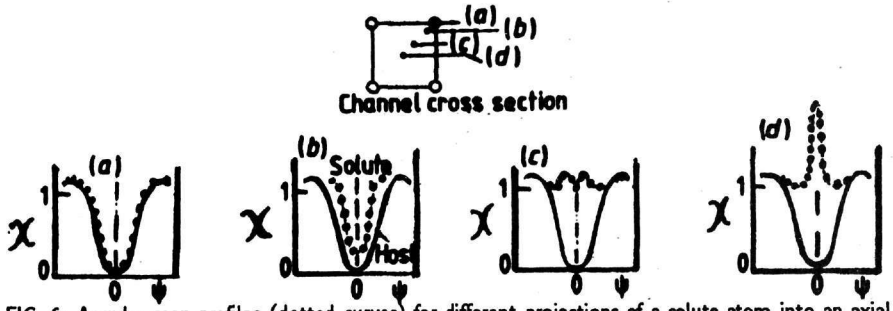

FIG. 6: Angular scan profiles (dotted curves) for different projections of a solute atom into an axial channel. The solid curve is the angular scan obtained when no solute atom is present (from ref. [2]).

which correspond to case c), a double peak can be seen. Case d) occurs when we deal with sites near the centre of the channel. In such a case, we find a pronounced narrow peak in yield from solute atoms. In fig. 7 an axial scan measured by means of the Goniometer system reported here is shown.

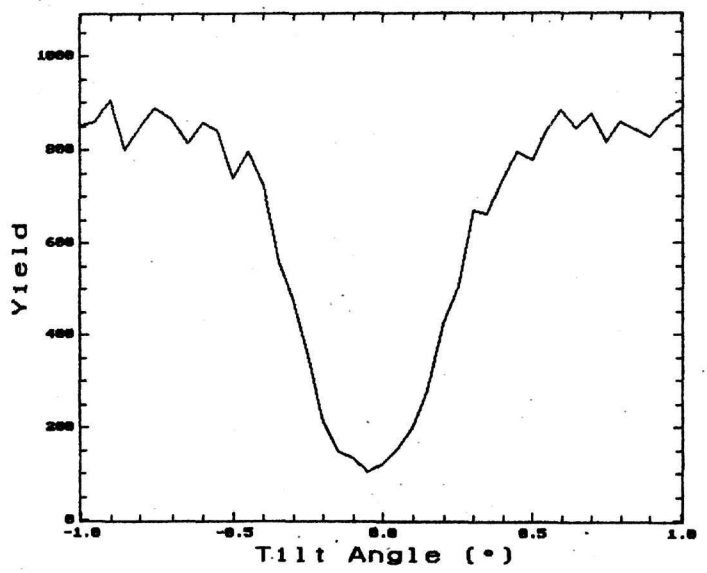

FIG. 7: Angular scan plot of a pure Si wafer measured with the Goniometer installed at "Demokritos".

2 Experimental procedures

2.1 THE SETUP

In order to carry out channeling measurements a special apparatus called *goniometer* is necessary. By means of the goniometer it is possible to find, with high accuracy, the appropriate orientation of the target sample to the beam axis, so that the beam particles "pass" through the crystal channels. This procedure is performed by tilting and/or rotating the target with respect to the beam, using stepping motors.

Recently, a "four axis" goniometer system has been installed at the Institute of Nuclear Physics of the Greek National Center for Scientific Research "Demokritos". The main parts of this system is manufactured by *Charles Evans and Associates* (*C.E.&A.*) It is consisted of following parts:

1. A vacuum chamber.
2. An RBS-50 Model 4-axis goniometer.
3. A motor controller and a motor driver (manufactured by *KLINGER*).
4. A laser system.
5. A personal computer (*HP Vectra/486/33 MHz*).

The vacuum chamber, in which the goniometer is mounted, is a 17-1/4 inch ID stainless steel cylinder. An horizontal cut of it is shown in fig. 8.

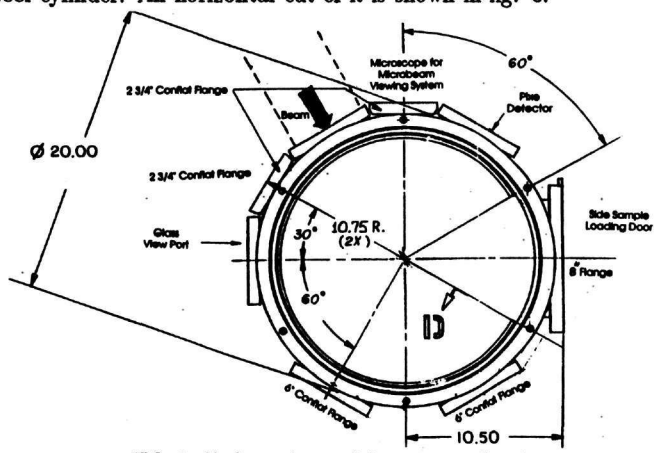

FIG. 8: Horizontal cut of the vacuum chamber.

The goniometer, which is integrated in the vacuum chamber, is shown in fig. 9. The target holder is a stainless steel cyclinder, which can be easily mounted on the goniometer through the loading door (see fig. 8). The arrows in fig. 9 indicate the possible tilts rotations and translations of the target holder. The $x-$tilt (see fig. 9) ranges from $-45°$ to $+45°$, whereas the $y-$tilt covers angles from $-90°$ to $+90°$.

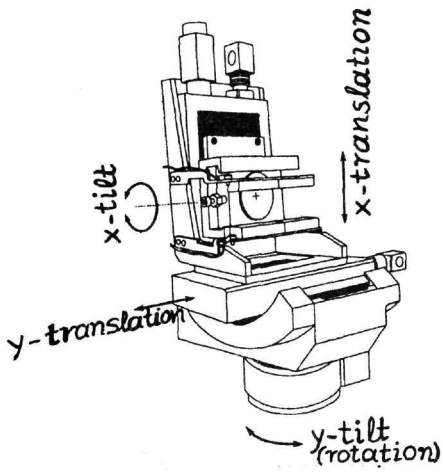

FIG. 9: The RBS-50 Model 4-axis goniometer of "Demokritos". The goniometer is placed in a vacuum chamber. The arrows indicate possible tilts, rotations and translations of the target holder.

The operation of the goniometer, i.e. the sample positioning, is achieved via 4 stepping motors driven by a motor power driver. The operation of power driver is controlled by a motor controller via an IEEE-488 interface. The motor controller, which is RS-232-C interfaced to the PC, can be operated via the *HYPRA* Software, developed by *C.E.&A.*. *HYPRA* controlls also beam current integration and data acquisition. The current integration is enabled by a beam current integrator coupled to a Counter Timer card (CTM-card), whereas the data acquitition proceeds by means of a Multichannel Analyzer card (MCA card). Both cards are resident in the PC. A block diagramm of the computer system and the electronics used is shown in fig. 10.

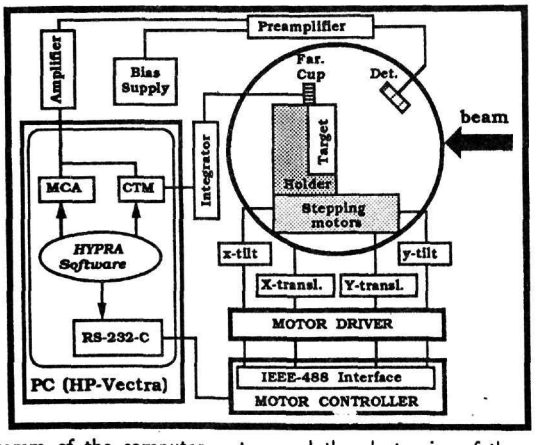

FIG. 10: Block diagramm of the computer system and the electronics of the goniometer system installed at "Demokritos".

The laser system is necessary to carry out following procedures before starting a measurement:

- **Alignment of the beam:** The laser beam is guided via a mirror system parallel the axis of the beam tube. The displacement of the laser beam from the beam tube axis is $\approx 1mm$. The beam before hitting the target is collimated by means of two sets of four Tantalum plates. Each of these plates can be translated vertical to the axis of beam tube by means of a micrometric screw. When beam and laser spot coincide then the beam is properly aligned.

- **Find the "eucentric point" of the target.** When this has been sucessfully done, then the beam or the laser spot does not "move" on the sample surface either up/down or left/right when tilting the target in any arbitrary angle.

- **Determine the coordinates of the samples.** These are needed by *HYPRA* to operate the motor controller, so that the samples are positioned properly to be hit by the beam.

A side view of the whole goniometer system as it is installed at "Demokritos" is given in fig. 11.

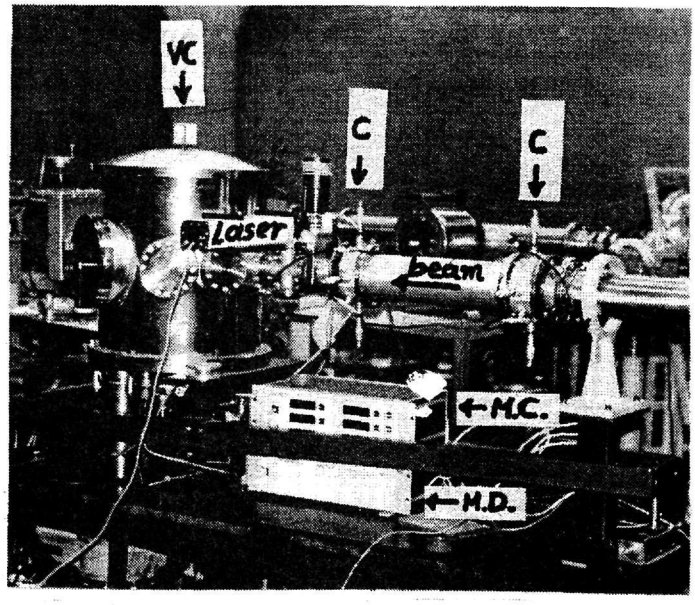

FIG. 11: Side view of the goniometer system installed at the Tandem lab of "Demokritos". C=Tantalum collimators, VC=Vacuum Chamber, M.D.=Motor Driver and M.C.=Motor Controller.

2.2 OBTAINING RBS-CHANNELING SPECTRA

In order to obtain channeling spectra following steps are usually followed.

Step 1: Encounter the channel.

After mounting the sample and positioning it randomly with respect to the beam axis, the orientation of the channel to be found can be roughly estimated by carrying out arbitrary $x-$ and $y-$tilts (see fig. 9) until the counting rate is decreased down to a minimum. When this has been occured, then according to the principles of channeling the sample has been aligned. In praxis, however, the beam has not been yet guided into the channel. *It simply encountered the channel*

Step 2: Perform a polar scan and obtain a polar scan plot.

In order to "guide" the beam particles into the channel of interest one has to "correct" the sample orientation achieved by step 1. This requires firstly to perform the so-called *Polar Scan*. By carrying out a Polar Scan one actually determines the orientation of the axis of a channel of interest with respect to the beam, i.e. the angles θ and ϕ between the channel axis and the beam axis. These angles are shown in fig. 12. They can be extracted

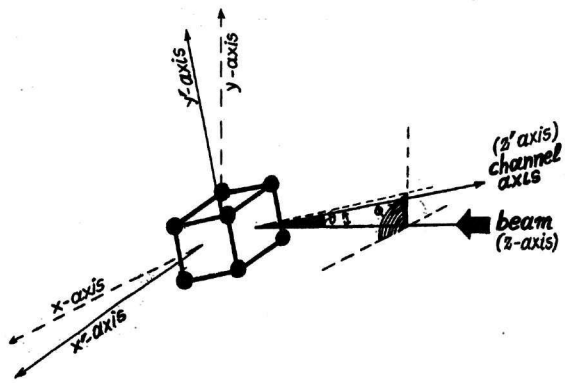

FIG. 12: Coordinate systems of a channel and the beam.

from the so-called *Polar Scan Plot* (PSP). Step 2 can be carried out via *HYPRA* software. Hereby, the analyst proceeds as follows:

1. The sample is firstly $y-$tilted to a small angle θ_t (typically $\theta_t = 5°$).

2. RBS counts are then measured for a given beam current at a preset number of different target orientations, i.e. at a preset number of different $y-$ and $x-$tilt pairs. For a given θ_t these pairs are calculated by *HYPRA* according to the following equations.

$$y_t = \theta_t \times cos(\phi) \tag{3}$$

$$x_t = \theta_t \times sin(\phi) \tag{4}$$

Angle ϕ ranges typically from 0° to 359° and it is "scanned" in 360 steps of 1° each. The range of ϕ as well as the step number are preset by the experimentator. An example of the sample orientations with respect to the beam is given by table 1. Hereby, the starting tilt angle θ_t has been preset to 5°, whereas ϕ runs from 0° to 359° in 360 steps of 1°

$\phi°$	$y_t°$	$x_t°$	$\phi°$	$y_t°$	$x_t°$	$\phi°$	$y_t°$	$x_t°$	$\phi°$	$y_t°$	$x_t°$
0	5.00	0.00	90	0.00	5.00	180	-5.00	0.00	270	0.00	-5.00
1	4.99	0.09	91	-0.09	4.99	181	-4.99	-0.09	271	0.09	-4.99
2	4.99	0.17	92	-0.17	4.99	182	-4.99	-0.17	272	0.17	4.99
...	.....	.....	...	.....	.....	...	.....	.....	...	.....	.....
89	0.09	4.99	179	-4.99	0.09	269	-0.09	-4.99	359	4.99	-0.09

Table 1: Typical y- and x-tilt pairs of the sample during a Polar Scan.

3. A Polar Scan Plot is obtained by plotting in a polar net the relative counting rates measured in a polar scan vs. the respective angle ϕ. In this polar net ϕ is chosen as the angular coordinate, whereas the counting rate is the radial coordinate. Fig. 13 shows a Polar Scan Plot obtained for an unimplanted Si-wafer. As it can be seen in this plot, there are some dips present, which according to the channeling principle correspond to crystal channels. However, due ω the symmetric $x-$ and $y-$tilting of the target with respect to the beam, one obtains *four minima for one channel.* Hence, by determining the coordinates of these dips, via next step, the orientation of the sample as been achieved by step 1, can be corrected so that the beam is guided properly into the channel of interest.

Step 3: Extract from Polar Scan Plot the spherical coordinates ϕ and θ of the channel axis with respect to the beam axis.

As already meantioned above, a Polar Scan Plot enables to determine the spherical coordinates ϕ and θ of a given channel axis with respect to the beam axis. The determination of ϕ and θ proceeds as follows:

1. As shown in fig. 13, by connecting the origin of the planar net with each of the four minima one obtains four different points: A, B, C, and D.

2. Points A, B, C, and D are further connected by two lines which intersect. Thus, one obtains point E.

3. The angular coordinate of this point, yields the angle ϕ between the axis of the channel of interest and the beam axis (see also fig. 11).

4. The respective spherical coordinate θ of the same channel axis is derived by multiplying the value of the radial coordinate of point E with the value of the tilt angle θ_t used to carry out the polar scan.

5. After angles ϕ and θ have been determined, *HYPRA* transforms their values into $x-$ and $y-$tilts for the sample and the target is positioned properly to measure channeling spectra.

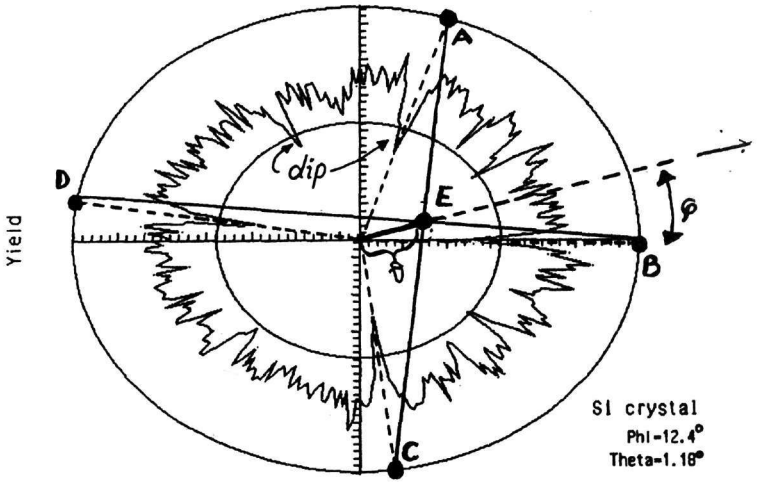

FIG. 13: Polar scan plot of an unimplanted Si wafer measured with the Goniometer installed at "Demokritos".

3 The first RBS and RBS-Channeling measurements

In this section some of the first RBS and RBS-Channeling measurements carried out via the goniometer system installed in "Demokritos" are presented. The order of these *demonstration measurements* is arbitrary.

Experiment 1: RBS-Channeling measurements of a BaBiCuO surface layer on a Si substrate using proton beams.

Some of the spectra measured in this experiment have been chosen for the present report in order to underline the importance of carrying out a Polar Scan as well as to demonstrate the high accuracy which can be achieved in target positioning by the goniometer installed at "Demokritos". The spectra considered are shown in in figs. 14 and 15. They have been measured by bombarding a thin BaBiCuO surface layer on a Si substrate with protons having an incident energy of 1.5 MeV.

Spectrum labeled "**a**" of fig. 14 is an angle scan measured after minimizing the counting rate, i.e. after step 1 (see section 2.2) has been carried out. As shown, however, by this angle scan a "deeper" minimum in counting rate arises at a different sample orientation: i.e. when the sample is additionally tilted to an angle $\theta \approx 2°$ with respect to the beam axis. Hence, the target is not "yet" properly aligned: As long as the minimum in the yield measured in an angle scan occurs not at $\theta = 0°$, the beam is still off channel

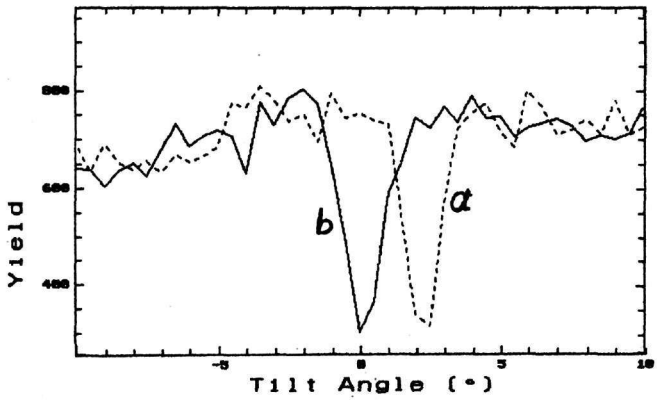

FIG. 14: Angle scans of a BaBiCuO surface layer bombarded with protons

axis. When beam axis and channel axis coincide, then instead of spectrum "a", one obtains an angle scan like this labeled "b". Hereby, the minimum is indeed arising at $\theta = 0°$. In order to obtain such an angle scan is necessary to carry out steps 2 and 3. How crucial these steps for channeling measurements are, is shown in fig. 15. In this fig., three different RBS spectra of the BaBiCuO layer considered are shown. Spectrum labeled "a" is this measured at the target orientation achieved by step 1, whereas spectrum "b" is this taken after steps 2 and 3 have been carried out. Clearly, spectrum "b" is a "channeled" spectrum, i.e. it is measured when beam axis and channel axis coincide. Furthermore, spectrum labeled "c" is a "random" spectrum, i.e. an RBS spectrum measured at a

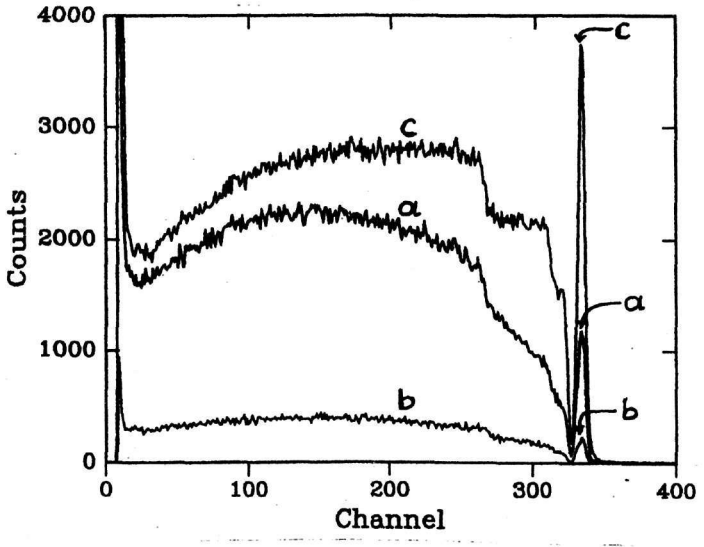

FIG. 15: RBS-spectra of a BaBiCuO surface layer bombarded with protons

random target orientation with respect to the beam. Spectra "a" and "b" of fig. 15 correspond to the target positions where angle scans "a" and "b" of fig. 14 have been measured. By comparing spectrum "a" with spectra "b" and "c", one can clearly see that although in case of spectrum "a" the angle between beam axis and channel axis was very small ($\theta \approx 2°$), this spectrum "deviates" from the channeled one "b" signifficantly. Spectrum "b" is rather "random alike". This "deviation" illustrates how crucial the "angle resolution" in target tilting could be in channeling measurements. The goniometer installed at "Demokritos" has an angle resolution in target tilting better than 0.01°. This value enables very accurate channeling experiments.

Experiment 2: RBS-Channeling measurements of an implanted Si wafer using α-beam.

In this experiment, α-particles having incident energy $E_\alpha = 2.5\ MeV$ have been used as a beam. The sample was a Si wafer. One half of its surface was implanted with BF_3 molecules (Dose=10^{15} moles/cm^2, Implantation-voltage=45 kV). The other half of its surface has been covered with an Al-foil during the implantation procedure. This enabled us to measure, using the same sample, the three different spectra shown in fig. 16. Spectrum labeled "a" is a random spectrum measured for the unimplanted part of

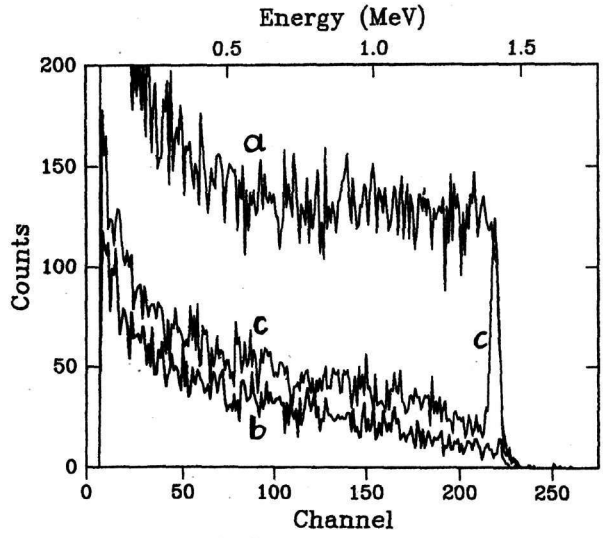

FIG. 16: RBS and RBS-Channeling spectra of a Si wafer. For explanations see text.

the sample. Spectrum "b" is the "channeled" spectrum taken with the unimplanted part of the sample, whereas spectrum "c" is the "channeled" spectrum of the implanted part of the wafer. The channel considered was the (100)-axis of the Si-crystal. The polar scan plot used to align the sample, i.e. to find the channel of interest is shown in fig. 13. As can be seen in fig. 16 a surface peak is present in spectrum "c". This peak arises due to some damage of the Si crystal surface occured during the implantation. This peak is "zoomed" in fig. 17.

The width ΔE_p of the surface peak present in spectrum "c" has been determined as $\Delta E_p = 36\ keV$. By taking into account that the energy resolution ΔE_d of the detector used was $\Delta E_d = 20\ keV$ one can derive (in keV units) the thickness t of the surface layer destructed via implantation as follows:

$$t_E = \sqrt{(\Delta E_p)^2 - (\Delta E_d)^2} = 30\ keV \tag{5}$$

Then t_E can be transformed in Å by taking into account that the energy loss dE/dx (in Si) of the α-particles having kinetic energy $E_\alpha = 2.5\ MeV$ is $dE/dx = 890\ keV/mg/cm^2$ and using the following equation for $\theta = 160°$ (detector angle):

$$t = \frac{t_E}{\frac{dE}{dx}(1 + \frac{1}{cos(\pi - \theta)})} = 700\ \mathring{A} \tag{6}$$

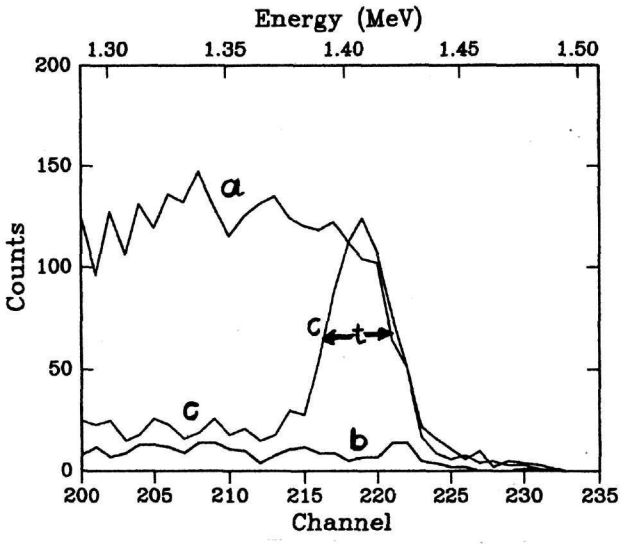

FIG. 17: Zoom in the RBS and RBS-Channeling spectra of a Si wafer shown in fig. 16. For explanations see text.

Experiment 3: RBS measurements of an YBaCuO superconducting surface layer on a MgO substrate via α beam.

In this measurement a thick MgO substrate layered by a YBaCuO superconducting film has been bombarded by α-particles of $E_\alpha = 2.5\ MeV$ incident energy. The "random" spectrum measured after 20 μCb beam charge is the "dotted" spectrum shown in fig. 18. The analysis of this spectrum via code *RUMP* [3] yielded a thickness $t = 1945$ Å for the YBaCuO layer as well as the following relative composition: Y:=1.0, Ba=1.845, Cu=2.365 and O=6.15.

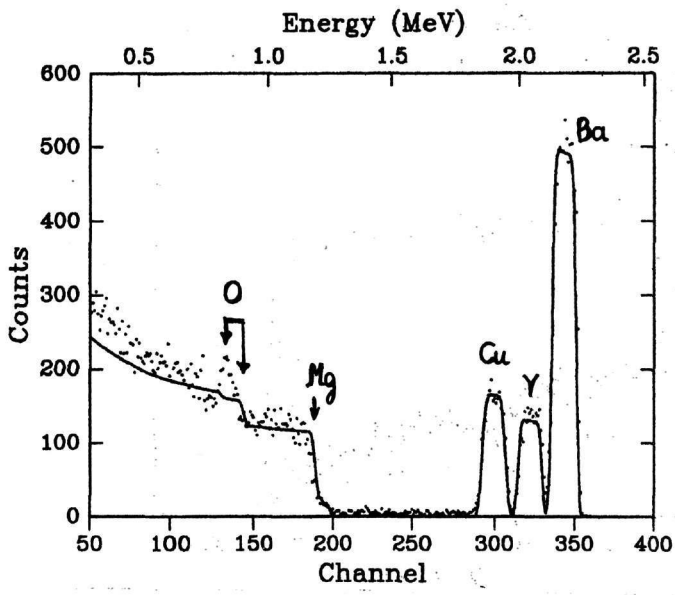

FIG. 18: Experimental ("dotted") and simulated ("solid") RBS spectrum of an YBaCuO superconducting layer on a thick MgO substrate.

The simulated spectrum, obtained by *RUMP*, is the "solid" spectrum shown in fig. 18. The deviation of the simulated spectrum from the measured one is a hint for some non-uniformity of the sample as well as for some oxigen concentration on the sample surface. To this deviation could also significantly contribute the yield of α-particles arising not from Rutherford backscattering but from the reaction $^{16}O(\alpha,\alpha')^{16}O'$.

Experiment 4: RBS measurements of a thick Si substrate layered by a Dy/Fe-alloy using α beam.

In this measurement an α-beam of incident energy of $2.5MeV$ was impinging on a thick Si-wafer with a layer of Dy- and Fe-atoms on his surface. The RBS-spectrum measured for this sample is shown in fig. 19. By analyzing this spectrum via code *RUMP*, the thickness t as well as the relative composition of the Dy/Fe layer could be determined. The analysis yielded a thickness $t = 15200$ Å and a relative composition Fe/Dy=0.73/0.27.

Experiment 5: RBS measurements with Carbon beam.

This experiment has been chosen here to demostrate the ability of the Tandem lab of "Demokritos" to analyse materials with a relative complex composition and using not only α or proton beams but also carbon beam.

The "dotted" spectrum shown in fig. 20 is an RBS spectrum of a sample delivered by the Institute of Solid State Physics of "Demokritos" with a rather complex (unknown) composition.

This sample has been bombarded via a carbon beam having incident energy $E = 10$ MeV. Using code *RUMP* the sample could be analysed as follows:

- **Layer 1:** Thickness t_1 = 7100 Å. Composition: Bi=0.9, Pb=0.2, Sr=1.8, Ca=1.8 Cu=3.5, O=17.0 and Fe=2.2.
- **Layer 2:** Thickness t_2 = 5000000 Å Composition: Mg=1.0, O=1.0 and Fe=0.2

By comparing the simulated ("solid") spectrum with the measured ("dotted") spectrum, shown both in fig. 20, one can clearly see that the analysis of the sample is rather sucessfull.

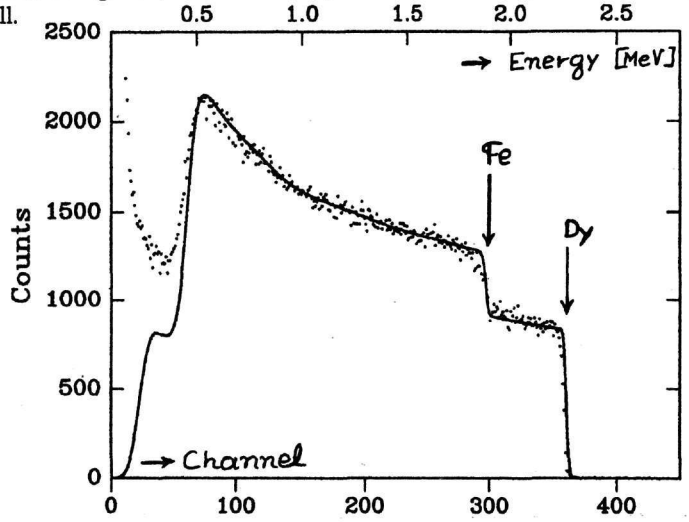

FIG. 19: Experimental ("dotted") and simulated ("solid") RBS-spectrum of a thick Si substrate with a Dy/Fe layer on its surface.

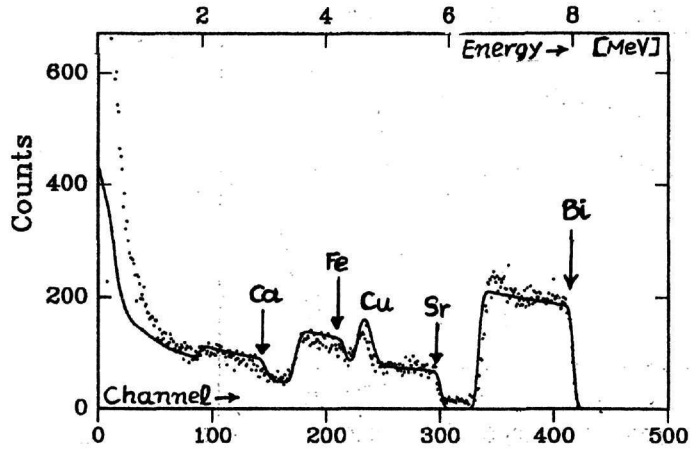

FIG. 20: Experimental ("dotted") and simulated ("solid") RBS-spectrum of a thick MgO substrate with a rather complex layer on its surface (see text).

4 Summary and Outlook

Summing up, the goniometer system installed recently at the Tandem laboratory of "Demokritos" is a rather modern and powerfull device to perform materials analysis. It enables to use the ion channeling technique additionally to the simple RBS method.

After the installation of the goniometer system presented in this report following topis in solid state physics and/or microelectronics can be studied at "Demokritos":

- Point defects
- Dislocations
- Stacking faults
- Mosaic structure
- Twinning
- Precipitates
- Strain
- Vibrations
- Impurities
- Crystal damage
- Crystal quality
- Epitaxy

References

1. L.C. Feldman, J.W. Mayer and S. Thomas Picraux, *Materials Analysis by ion channeling*, (Academic Press, New York, 1982)
2. M.L. Swanson, Rep. Progr. Phys, **45**(1982)47
3. Code *RUMP*, L.R. Doolittle, Nucl. Instr. Meth. **B9** (1985)344, and Nucl. Instr. Meth. **B15**(1986)227